Development of 3D-printed subcutaneous implants using concentrated polymer/drug solutions

International Journal of Pharmaceutics 631 (2023) 122477

Contents lists available at ScienceDirect

International Journal of Pharmaceutics

journal homepage: www.elsevier.com/locate/ijpharm

Development of 3D-printed subcutaneous implants using concentrated polymer/drug solutions

Camila J. Picco [a], Emilia Utomo [a], Andrea McClean [a], Juan Domínguez-Robles [a], Qonita Kurnia Anjani [a], Fabiana Volpe-Zanutto [a], Peter E. McKenna [a], Jonathan G. Acheson [b], Dessislava Malinova [c], Ryan F. Donnelly [a], Eneko Larrañeta [a,*]

[a] School of Pharmacy, Queen's University Belfast, 97 Lisburn Road, Belfast BT9 7BL, United Kingdom
[b] Nanotechnology and Integrated Bioengineering Centre (NIBEC), School of Engineering, Ulster University, United Kingdom
[c] Wellcome-Wolfson Institute for Experimental Medicine, Queen's University Belfast, Belfast, United Kingdom

ARTICLE INFO

Keywords:
Olanzapine
Poly(caprolactone)
Poly(ethylene)glycol
Implant
3D printing
Sustained delivery

ABSTRACT

Implantable drug-eluting devices that provide therapeutic cover over an extended period of time following a single administration have potential to improve the treatment of chronic conditions. These devices eliminate the requirement for regular and frequent drug administration, thus reducing the pill burden experienced by patients. Furthermore, the use of modern technologies, such as 3D printing, during implant development and manufacture renders this approach well-suited for the production of highly tuneable devices that can deliver treatment regimens which are personalised for the individual. The objective of this work was to formulate subcutaneous implants loaded with a model hydrophobic compound, olanzapine (OLZ) using robocasting - a 3D-printing technique. The formulated cylindrical implants were prepared from blends composed of OLZ mixed with either poly(caprolactone) (PCL) or a combination of PCL and poly(ethylene)glycol (PEG). Implants were characterised using scanning electron microscopy (SEM), thermal analysis, infrared spectroscopy, and X-ray diffraction and the crystallinity of OLZ in the formulated devices was confirmed. *In vitro* release studies demonstrated that all the formulations were capable of maintaining sustained drug release over a period of 200 days, with the maximum percentage drug release observed to be c.a. 60 % in the same period.

1. Introduction

Pharmacological management of chronic conditions, such as HIV or schizophrenia, typically requires regular and frequent drug administration to ensure positive therapeutic effects are achieved (Larrañeta et al., 2022). Unfortunately, this means that drug regimens for chronic conditions are associated with significant pill burdens and, as a consequence, their success is heavily reliant on the extent to which a patient can comply to their demanding drug regimen. In many instances, treatment non-adherences is seriously impactful upon the quality of life of many patients and in some cases can result in premature mortality (Kleinsinger, 2018). For example, research has demonstrated that poorly compliant schizophrenic patients have a higher relapse rate which, in turn, is associated with higher rates of hospitalisation and suicide (Higashi et al., 2013). Whilst such patient-centred impacts are of utmost importance, they are not the only concerning outcome stemming from treatment non-adherence in the case of chronic health conditions. Regrettably, the economic impact that treatment non-adherence places on health systems across the globe, in the form of increased hospital admissions and resource wastage leading to heightened treatment costs, can be felt in almost all aspects of healthcare (Cutler et al., 2018). Accordingly, there is a clear un-met need for alternative drug delivery systems that reduce the demands of treatment regimens for chronic conditions, thus rendering them more patient-friendly with an associated ease of adherence.

A potential alternative for the treatment of chronic conditions is the development of long-acting implantable devices (Corduas et al., 2020; Larrañeta et al., 2022; Stewart et al., 2021). These devices are internally embedded (usually in lower layers of the skin) and possess the ability to release drug in a controlled manner over an extended period of time following a single administration (Larrañeta et al., 2021). As a result, these devices eliminate the requirement for regular and frequent drug

* Corresponding author at: School of Pharmacy, Queen's University Belfast, 97 Lisburn Road, Belfast BT9 7BL, UK.
E-mail address: e.larraneta@qub.ac.uk (E. Larrañeta).

https://doi.org/10.1016/j.ijpharm.2022.122477
Received 10 September 2022; Received in revised form 2 December 2022; Accepted 5 December 2022
Available online 9 December 2022

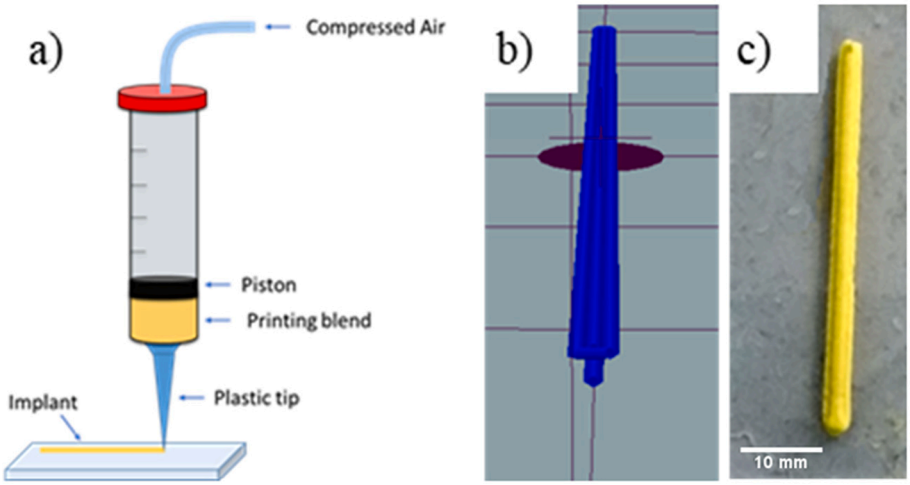

Fig. 1. a) Representative diagram of how the Allevi® 3D Bioprinter works, b) Implant design on the Repetier-Host programme after slicing function producing two layers each 0.6 mm high, c) OLZ-PCL-PEG implant printed using the 20-gauge tip.

administration, thus greatly reducing the pill burden associated with a given therapeutic regimen. Additionally, due to the avoidance of first-pass metabolism and the harsh environments of the gastrointestinal tract (enzymatic degradation and fluctuations in pH) following administration, drug delivery in this manner may translate into improved drug bioavailability and, therefore, reduced incidence of dose-related toxicity (Fialho and Silva Cunha, 2005).

Implantable devices can be prepared using a wide variety of techniques and materials (Quarterman et al., 2021; Utomo et al., 2022b). Recently, the use of additive manufacturing (also known as 3D printing), which is a set of manufacturing techniques based on the deposition of material layer by layer for the building of a 3D object, has been utilised to great effect for this purpose (Domsta and Seidlitz, 2021). Previously, 3D printing has been explored for the design and manufacture of many drug delivery systems including suppositories (Seoane-Viaño et al., 2021) and oral tablets (Awad et al., 2020; Lopez-Vidal et al., 2022; Melocchi et al., 2020; Pandey et al., 2020; Tian et al., 2018). However, it has shown particular promise in the development of implantable medical devices, such as wound dressings (Teoh et al., 2021), surgical meshes (Domínguez-Robles et al., 2020; Farmer et al., 2021, 2020), cardiovascular grafts (Domínguez-Robles et al., 2022, 2021b,2021a; Kabirian et al., 2018; Martin et al., 2021; Melchiorri et al., 2016) and subcutaneous implants (Korelidou et al., 2022; Liaskoni et al., 2021; Ruiz-Cantu et al., 2022; Stewart et al., 2020a; Stewart et al., 2020b). Not only is the use of 3D printing to fabricate implants affordable and easy, but this technique is highly tuneable in nature with the ability to produce personalised formulations containing multiple drugs at varying concentrations tailored to the needs of a given patient (Khaled et al., 2014; Stewart et al., 2020a).

The work reported within details the development and characterisation of 3D-printed polymeric implants composed of poly(caprolactone) (PCL), poly(ethylene)glycol (PEG) or a combination of both polymers, loaded with the second-generation antipsychotic drug olanzapine (OLZ) as a model compound. In this work, 3D-printing in the form of robocasting (also known as robotic material extrusion) was used to combine polymer(s) with OLZ and form individual implants in a manner consistent with additive manufacture. Following this, the physicochemical properties of the resultant implants were evaluated using multiple techniques, such as scanning electron microscopy (SEM), differential scanning calorimetry (DSC), thermogravimetric analysis (TGA), Fourier-transform infrared (FTIR) spectroscopy and X-ray micro-computed tomography. Finally, drug release from and the cytocompatibility of the formulated implants were evaluated in an *in vitro* setting.

Table1
Formulations of the different implants tested.

Formulation	Content in the dry state (% w/w)		
	OLZ	**PCL**	**PEG**
OP5	50	50	–
P	–	100	–
OPP5	50	30	20
PP	–	60	40
OPP8	80	12	8

2. Materials and methods

2.1. Materials

OLZ powder was provided by Cangzhou Enke Pharma-tech Co. ltd. (Coleshill, Warwickshire, UK). PEG (MW = 3,000 Da), Dichloromethane (DCM) and Acetonitrile (ACN) were obtained from Sigma-Aldrich (Gillingham, Dorset, UK). PCL - CAPA^{TM} 6505 (MW = 50 000 Da, *i.e.,* high molecular weight) was obtained from Ingevity (North Charleston, South Carolina, U.S.A). Acetic acid was obtained from Honeywell International Inc. (Charlotte, North Carolina, U.S.A) and sodium azide was obtained from Fluorochem ltd. (Hadfield, Derbyshire, UK).

2.2. Implant design and manufacture

To facilitate implant manufacture *via* 3D printing, drug-containing solutions with varying compositions were prepared by dissolving OLZ, PCL and PEG at different concentrations in a minimum volume of DCM. To ensure content homogeneity, solutions were mixed at 3000 rpm for 3 min using a SpeedMixer™ DAC 150.1 FVZ-K (Hauschild GmbH & Co. KG, Westfalen, Germany). Following mixing, solutions were loaded into a 10 mL plastic syringe with a 20-gauge tip which was then attached to the 3D printer head. Each implant was designed using computer-aided design (CAD) software, Tinkercad® and printed using an Allevi® 2 Bio-printer, a material extrusion-based technology (Fig. 1), at ambient lab conditions. Print speed was maintained at 2 mm/s, layer height was 0.6 mm and nozzle pressure was 38 psi. Individual implants were of cylindrical shape with length and diameter of 50.0 mm and 1.5 mm, respectively. Upon print completion, implants were dried in a fume hood (*i.e.,* solvent was evaporated) under ambient lab conditions for 3 days. Drug-free implants were also prepared following the same methodology. The final composition of the dry implants prepared can be seen in Table 1. It may be worth noting that less DCM (57–60 %) was needed to

prepare OP5 and OPP5, compared to OPP8 (73 %), as the latter formulation possessed a higher drug loading and, therefore, required more solvent to solubilise OLZ.

2.3. Physicochemical characterisation of implants

2.3.1. Microscopic examination

The formulated implants were examined using a Leica E24W digital microscope (Leica, Wetzlar, Germany). Furthermore, implant morphology was examined using a Tabletop scanning electron microscope (SEM) (Hitachi TM3030, Tokyo, Japan). SEM analyses were carried out without sample pre-treatment using a voltage of 15 kV in low vacuum mode.

2.3.2. Differential scanning calorimetry and thermogravimetric analysis

Individual implants and the raw materials from which they were made were analysed using a Q100 differential scanning calorimeter (TA Instruments, Bellingham, WA). Scans were performed from 25 °C to 225 °C with a heating rate of 10 °C/min under a constant flow of nitrogen (50 mL/min). To further characterise the same materials, a Q500 Thermogravimetric analyser (TA Instruments, Bellingham, WA) was used. During these analyses, samples were heated from 25 °C to 500 °C at a rate of 10 °C/min under a nitrogen flow rate of 40 mL/min.

2.3.3. Attenuated total reflectance Fourier transform- infrared spectroscopic analysis

The Fourier transform infrared spectra of the implants and the raw materials from which they were prepared were recorded using a Spectrum Two FT-IR Spectrometer (Perkin Elmer, Waltham, MA) equipped with a MIRacle™ diamond attenuated total reflectance (ATR) accessory (PIKE technologies, Fitchburg, MA). Each spectrum was recorded from 4000 cm^{-1} to 600 cm^{-1} with a resolution of 4 cm^{-1} with an average of 32 scans collected.

2.3.4. Powdered X-ray diffraction

To evaluate the crystallinity of the formulated implants and their starting materials, each was analysed using a MiniFlex™ X-ray powder diffractometer (Rigaku Corporation, Tokyo, Japan) equipped with Ni-filtered, Cu Kβ radiation and a voltage of 30 kV. Scanning was performed at a rate of 2.0°/min across an angular range of 3-60° 2θ (2 thetas) in continuous mode with a sampling width of 0.03°at room temperature. The current used was 15 mA and the voltage was 30 kV as described in previous work (Anjani et al., 2022; Volpe-Zanutto et al., 2021).

2.3.5. Micro-computed tomography

Micro-Computed Tomography (μCT) analysis was conducted using a Bruker Skyscan 1275 (Bruker, Germany), operating at 25 kV and 125 μA with an image pixel size of 8 μm. Rotational images were translated into 2D slices using NRecon (Bruker, Germany). Maximum Intensity Projection (MIP) reconstructions were then created using CTVox (Bruker, Germany). MIP reconstructions allow for the identification and display of entities of higher density within a given volume.

2.3.6. Drug quantification using high performance liquid chromatography

OLZ was quantified using reverse-phase high-performance liquid chromatography (RP-HPLC) (Agilent 1100 series system, Agilent Technologies UK ltd., Stockport, UK) as reported previously (Picco et al., 2022). The column used to achieve separation was a Waters X-Select CSH C18 (3.5 μm pore size, 3.0 × 150 mm) (Agilent Technologies UK ltd., Stockport, UK). Mobile phase composition was ACN and de-ionised water (pH: 2.3) at a ratio of 60:40, with a flow rate of 0.5 mL/min, injection volume of 10 μL and a sample runtime of 5 min. Ultraviolet (UV) detection was carried out at a wavelength of 260 nm.

2.4. Drug release from implants

To evaluate the rate and extent of drug release from the formulated implants over a period of 200 days, individual devices were placed into glass flasks containing 50 mL PBS (pH: 7.4) and incubated at 37 °C ± 1 °C with agitation set at 40 rpm. To prevent growth of microorganisms within the release media, sodium azide at a concentration of 0.1 % v/v was added. At pre-determined and regular timepoints, 1 mL samples of the media were taken and analysed using RP-HPLC, as described previously (Picco et al., 2022). Following this, the volume of receiver media was replenished with 1 mL of fresh PBS containing sodium azide to ensure consistency. Additionally, the solubility of OLZ in PBS at 37 °C was determined and this value was used to ascertain when release media needed to be replaced to ensure that the experiment was carried out under sink conditions at all times. The Korsmeyer-Peppas kinetic model were used to characterise the release behaviour of each formulation (Costa and Sousa Lobo, 2003; Larrañeta et al., 2014; Ritger and Peppas, 1987). Specifically, data obtained from release experiments were analysed using Equation (1).

$$Q_t/Q_\infty = K_{KP}t^n \quad (1)$$

Q_t represents the amount of drug released at time t and Q_0 is the amount of drug in the matrix. The Korsmeyer-Peppas release constant is represented by K_{KP}. The value of the exponent n depends on the drug release mechanism (Costa and Sousa Lobo, 2003; Larrañeta et al., 2014; Ritger and Peppas, 1987). An exponent value of $\leq$ 0.5 indicates that drug release follows a Fickian diffusion model. Whereas, an exponent value between 0.5 and 1 or $\geq$ 1 suggests non-Fickian (also called anomalous) transport or case II transport, respectively.

2.5. Residual solvent content

To determine residual solvent content of the formulated implants, an Agilent 7820A gas chromatographer (Agilent Technologies UK ltd., Stockport, UK) equipped with a 7697A Headspace autosampler and an FID detector and an Agilent 19091 J-413 (30 m × 320 μm × 0.25 μm) column was used. Throughout analysis, column, injector and detector temperatures were maintained at 40 °C, 250 °C and 300 °C, respectively. The sample was injected onto the column using a split ratio of 10:1 with a flow rate of 1 mL/min and a total run time of 3 min.

2.6. Cytocompatibility of implants

HEK293T cells (human embryonic kidney, ATCC) were seeded in a 24-well plate (30,000 cells/well) and cultured with Dulbecco's modified Eagle medium (DMEM) and 10 % fetal calf serum with non-essential amino acids. Following overnight incubation, an equal volume of culture media was incubated in direct contact with a section of an implant. On day 3 of co-culture, a cell viability test using an MTT staining method (3-(4,5-dimethylthiazol-2-yl)-2,5-diphenyltetrazolium) was conducted. Cells were washed with PBS, then MTT solution was added to each well and the plate was further incubated at 37 °C for three hours. Absorbance at a wavelength of 570 nm was calculated in triplicate for each sample using a plate reader (Biotek, Winooski, VT). In this assay, viable cells are able to convert water-soluble MTT to an insoluble formazan product, which results in a coloured precipitate that is quantifiable by spectrophotometry (Elamparithi et al., 2016; Serrano et al., 2004). Untreated cells and cells treated with 4 % paraformaldehyde for 15 min were used as positive and negative controls, respectively.

2.7. Statistical analysis

Where appropriate data was expressed as the mean ± standard deviation. Data from cytocompatibility studies were compared using one-way ANOVA with Tukey's HSD post hoc analysis. In all cases, a p value

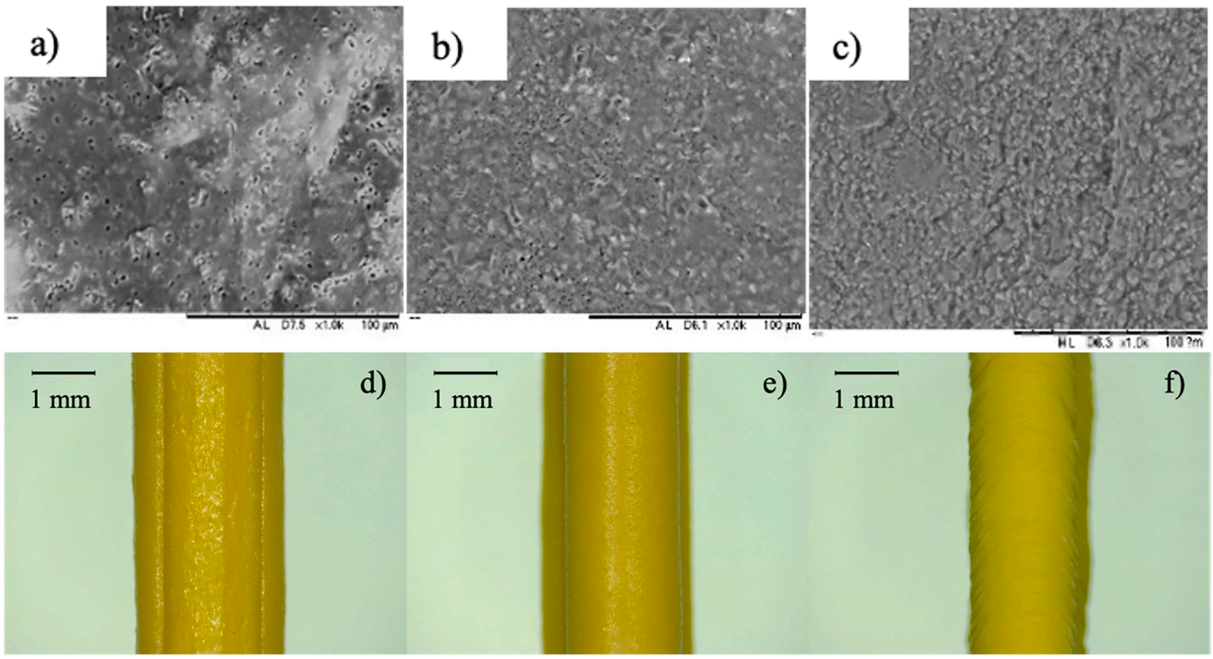

Fig. 2. SEM photomicrographs of the formulated implants at x1000 magnification - a) OP5, b) OPP5 and c) OPP8. The scale in these images is 100 μm. Images of the formulated implants using the Leica E24W microscope at x16 magnification d) OP5 implant, e) OPP5 implant and f) OPP8 implant.

< 0.05 indicated a statistical significance.

3. Results and discussion

3.1. Implant design and manufacture

Rod-shaped implants with dimensions measuring 1.5 mm in width and 50 mm in length were printed using an Allevi®2 Bio-printer (Fig. 1). This design was chosen as it is similar to other implants that have been successfully marketed and are currently commercially available (Funk et al., 2005; Stewart et al., 2020). As described previously, implants were polymeric in composition and were loaded with the antipsychotic drug OLZ as a model compound. During this developmental work, two different polymer compositions (PCL and a mixture of PCL and PEG), as well as two different drug loadings (50 % and 80 %) were tested. Previous studies suggest that the inclusion of hydrophilic excipients may accelerate drug release and, therefore, to further explore this phenomenon the water-soluble polymer PEG was incorporated into the implant matrix to evaluate its effect on drug release kinetics. To facilitate implant formation *via* robocasting, formulation components (*i.e.,* OLZ and the required polymers) were dissolved in DCM at high concentrations to produce a printable OLZ-containing polymeric slurry. Following printing, DCM was evaporated from the printed object under ambient lab conditions to form solid drug-containing implants. This approach has been used in the past with aqueous mixtures for the development of solid oral dosage forms and implantable devices (Khaled et al., 2018a; Khaled et al., 2018b; Picco et al., 2022). One of the key advantages of 3D-printing over conventional manufacturing techniques is that can be used to prepare highly personalised drug delivery systems (Vaz and Kumar, 2021). Accordingly, as the formulated implants have been prepared using 3D-printing, they too can be easily modified to suit the needs of a patient at the point of care. Due to their mechanism of action, implantable devices are required to be sterile prior to use. Therefore, unless implants are prepared under sterile conditions, a terminal sterilisation process must be used to meet this requirement. Currently, sterilisation by exposure to gamma radiation or ethylene oxide are considered by many to be the most promising techniques ("Ethylene oxide sterilization: how hospitals can adapt to the changes.," 1994). However, regardless of chosen sterilisation strategy the properties of the resultant device, *i.e.,* toxicity risk and drug release kinetics, must not be altered.

The robocasting method proposed here possesses an additional advantage over conventional 3D-printing techniques, such as fused deposition modelling, as it does not require the use of high temperatures. With this approach both the drug and polymer(s) are dissolved or suspended in the solvent matrix and, therefore, the addition of heat to melt polymer is not required. This is, of course, viewed favourably as many active pharmaceutical ingredients are readily degraded by heat *i.e.,* thermolabile. Additionally, the use of a solvent in which both the polymer(s) and drug are soluble facilitates enhanced drug loading capabilities whilst ensuring an unproblematic printing process (Khaled et al., 2018; Picco et al., 2022). With conventional 3D-printing techniques, drug loading is typically no greater than 50 % with a majority of reports stating figures between 20 and 30 % (Cailleaux et al., 2021). Yet, with the approach reported here, a drug loading of 80 % has been achieved with relative ease.

Regarding the selection of polymers for implant fabrication, PCL was selected as it is both biocompatible and biodegradable and it has been used previously in the development of implants for sustained drug delivery (Barrett et al., 2018; Boia et al., 2019; Stewart et al., 2021). It should be noted that the degradation rate of PCL is not as fast as PLGA (another polymer commonly used in the fabrication of implants), which is regrettable as this may result in patients who suffer from chronic conditions needing to have their implants removed following drug cargo depletion. However, this will not be an issue for patients that require a single implant to fulfil their treatment needs *i.e.,* antimicrobial prophylaxis, pain management after surgery or localised cancer treatment. Additionally, with all polymers, but particularly PLGA, appropriate selection based on the reliability of polymer degradation rate is an absolute requirement as faster degradation of the implant matrix can contribute to accelerated drug release at later stages of implant lifecycles (Bassand et al., 2022; Lao et al., 2008).

3.2. Physicochemical characterisation of implants

The morphology of the formulated implants was evaluated using

Table 2
Dimensions, weight and drug content of the formulated implants.

Implant	Length (mm)	Width (mm)	Height (mm)	Weight (mg)	Drug content (mg)
OP5	48.2 ± 0.1	3.6 ± 0.1	1.6 ± 0.1	254 ± 8	127 ± 4
OPP5	47.8 ± 0.1	2.6 ± 0.1	2.1 ± 0.1	211 ± 2	105 ± 1
OPP8	48.3 ± 0.4	2.1 ± 0.4	2.0 ± 0.2	198 ± 22	158 ± 18

SEM (Fig. 2a-c) and a digital microscope (Fig. 2d-f). Light microscope images showed that the implants presented a relatively homogeneous structure. SEM was used to evaluate if the drug was evenly distributed in the implant. All 3D-printed implants possessed a rough surface. Images show no obvious accumulation of the drug and that it is uniformly spread throughout. These results suggest that OLZ has well dispersed within the different polymeric matrices either PCL or the combination of PCL and PEG. The yellow colour of the implants confirms the presence of OLZ (Fig. 2d-f). Inspection of the formulated implants using SEM re-enforced the belief that OLZ was uniformly distributed within both the PCL and PCL-PEG matrices no evidence of OLZ aggregation was observed. Therefore, it was assumed that the mixing process, a dual

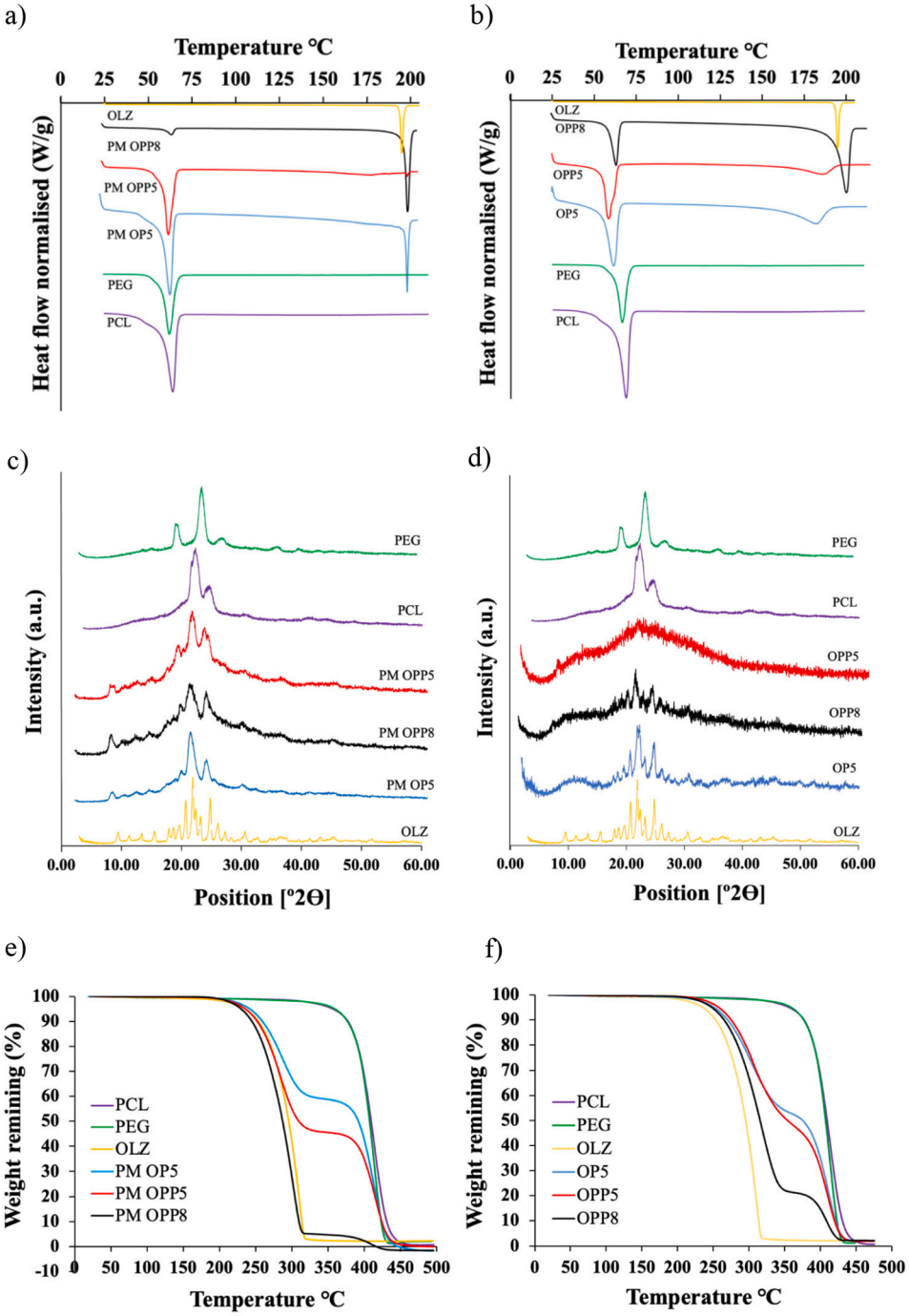

Fig. 3. DSC traces for (a) physical mixtures (PM) and (b) OLZ-loaded implants. XRD diffractograms for (c) physical mixtures (PM) and (d) OLZ-loaded implants. TGA curves for (e) physical mixtures (PM) and (f) OLZ-loaded implants.

asymmetric centrifugal laboratory mixer system, performed successfully.

The dimensions, weight and drug content of the formulated implants is presented in Table 2. Implants prepared using the technique described in this work possessed consistent length (approx. 48 mm). On the other hand, implant width and height was highly dependent on formulation composition. For example, due to extensive formulation spreading before drying OP5 implants presented higher width than height. This phenomenon is quite common when printing using gels and viscous materials (Kyle et al., 2017). However, formulation spreading did not occur to the same extent with OPP5 and OPP8 implants, which suggested that the incorporation of PEG improved formulation printability.

Formulating a drug into an implant in this manner may result in interactions between polymer(s) and the drug (Champeau et al., 2015). To determine whether such interactions had occurred with OLZ in this instance, the formulated implants and the raw materials from which they are prepared were extensively characterised and, subsequently, compared to detect any changes that may indicate interaction occurrence. Regarding the raw materials from which the implants were prepared, the melting point peak of OLZ was observed at approximately 195 °C, which was significantly higher than those of PCL and PEG (both of which were observed at approximately 60 °C) (Fig. 3**a-b**). These results, therefore, indicated that both OLZ and the polymers (PCL and PEG) used to prepare the implants possessed a certain degree of crystallinity. Considering the DSC traces of the formulated implants (Fig. 3**b**), it is evident that, in each case, the endothermic peak of OLZ was broader than the peak observed in OLZ alone. Moreover, in implants that were loaded with OLZ at a concentration of 50 % w/w (OP% and OPP5) the same peak had shifted to a temperature lower than 195 °C. These findings indicated that the formulation of polymeric drug-containing implants in the manner described within considerably reduced drug crystallinity, which correlates with enhanced drug solubility. In support of this hypothesis, it can be seen in Fig. 3a that the traces of all physical mixtures possessed a sharp OLZ melting point peak that cannot be seen in the traces of the formulated implants. Moreover, these data also indicate that the inclusion of PEG in an implant induced a higher reduction in OLZ crystallinity. These findings are in agreement with those reported by Picco et al. and Pina et al. where a similar phenomenon was observed by combining OLZ with poly(ethylene)oxide (Picco et al., 2022) or poly(vinyl pyrrolidone) (Pina et al., 2014).

XRD diffractograms of pure OLZ, PCL and PEG, as well as the formulated implants and their corresponding physical mixtures are presented in Fig. 3**c-d**. Drug crystallinity when formulated into an implant was assessed by comparing peaks observed on the diffractograms of implants and physical mixtures with the crystalline peaks observed on the diffractogram of pure OLZ. The diffractogram of OLZ displayed several sharp peaks at angles of 20.76°, 21.94°, 23.22°, 24.64°, 24.82° and 26.14°, which confirmed the crystallinity of the drug in its unprocessed form. When OLZ was formulated into implants containing PCL only (OP5), these crystalline peaks were still present. This finding, combined with the shift in the melting point peak observed during DSC analysis, suggest that while the structure of OLZ present in these implants was increasingly amorphous, there was still some crystallinity present. This phenomenon was not observed on the diffractogram of implants with similar drug loading *i.e.,* 50 %, where PCL and PEG were used (OPP5). In this case, all of the crystalline peaks observed on the diffractogram of pure OLZ had disappeared, which indicated complete conversion of OLZ into an amorphous form. When OLZ concentration was increased to 80 % (OPP8), the drug's crystalline peaks returned once again which indicated that there was insufficient polymer available to interact with all of the OLZ and, thus, a portion of the drug remained in its crystalline form. The findings obtained here align with those acquired from DSC analyses.

Further confirmation of the occurrence of drug/polymer interactions was achieved through TGA analysis (Fig. 3**e-f**). Two clear degradation stages could be seen in the samples of OP5, OPP5 and OPP8 implants.

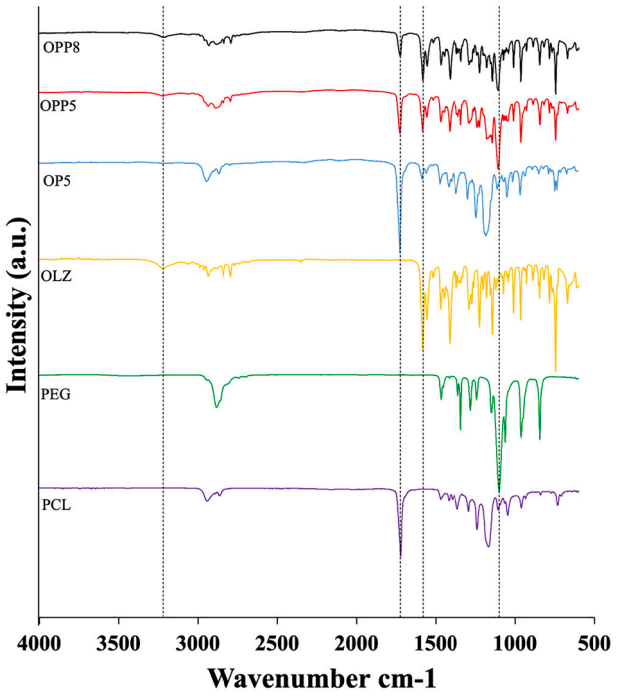

Fig. 4. FTIR spectra of OPP8, OPP5 and OP5 implants, in addition to pure OLZ, PEG and PCL powders showing percentage transmittance over wavenumber range (4000–600 cm^{-1}).

These stages overlap as the first decomposition reaction is not complete before the second one starts. The first peak is attributed to OLZ degradation (233.92 °C) while the second is of the polymer(s) (PCL 350.95 °C and PEG 344.29 °C). Interestingly, TGA curves for implants showed different degradation profiles than the physical mixtures. The degradation process of the implants starts at lower temperatures than in the physical mixtures. This could be attributed to the presence of a higher amount of amorphous OLZ which is less stable than its crystalline form. This trend can be seen clearly for OP5 and OPP5. The latter presents higher weight loss attributed to OLZ degradation than OP5 due to the amorphous nature of OLZ within OPP5.

FTIR analysis was performed (Fig. 4) to establish the interactions observed during DSC, XRD and TGA analysis. The spectra of implants and the individual components from which they were made were compared to determine if the preparation of implants resulted in any drug/polymer interactions. Peaks characteristic of OLZ, such as the peak at 3200 cm^{-1} corresponding to the N—H bonds and 1583 cm^{-1} to the C═C bonds, were present in both the spectra of unprocessed OLZ powder spectra and OLZ-containing implants. This confirmed successful incorporation of OLZ into the matrix of the formulated implants (Hiriyanna et al., 2008). Peaks characteristic of PCL, including the peak at 1723 cm^{-1} corresponding to the C═O bond of an ester (Danafar et al., 2014), and PEG, such as the peak at 1099 cm^{-1} corresponding to C—H bonding, are also present in the implants (León et al., 2017). In this work, peak shifts are considered to be indicative interactions between the drug and polymer or between the two polymers. Accordingly, the peak at 1723 cm^{-1} presents peak shifts in the spectra of all implants tested. Considering that OLZ contains an N—H group it is plausible to suggest that H-bonding is taking place between the C═O on PCL and the N—H on OLZ. This hypothesis is supported by the observation of a slight peak shift for the OLZ N—H band at around 3200 cm^{-1}. Interestingly, it is possible that hydrogen bonding may take place between C—O—C groups in PEG and the N—H group in OLZ. This hypothesis is consistent with the peak shift of the 1099 cm^{-1} band observed for OPP5 implants. These polymer/drug interactions, which have now been extensively characterised, contribute to OLZ amorphisation. Finally, the fact that no

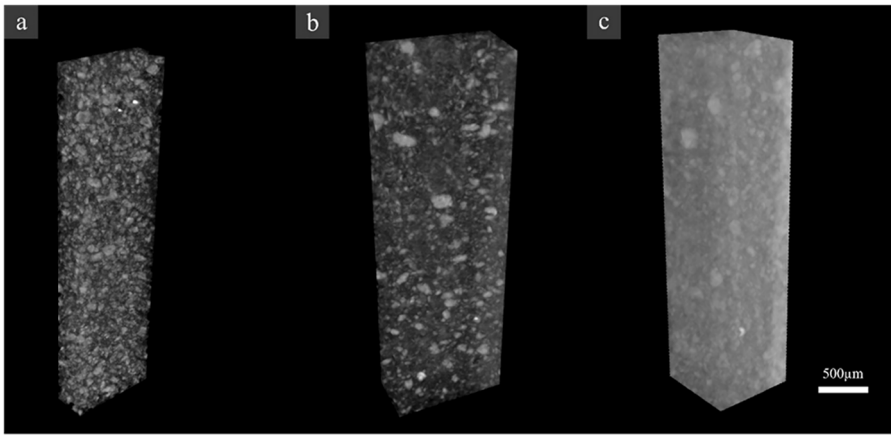

Fig. 5. Maximum intensity projection µCT reconstructions of OP5 (a), OPP5 (b) and OPP8 (c).

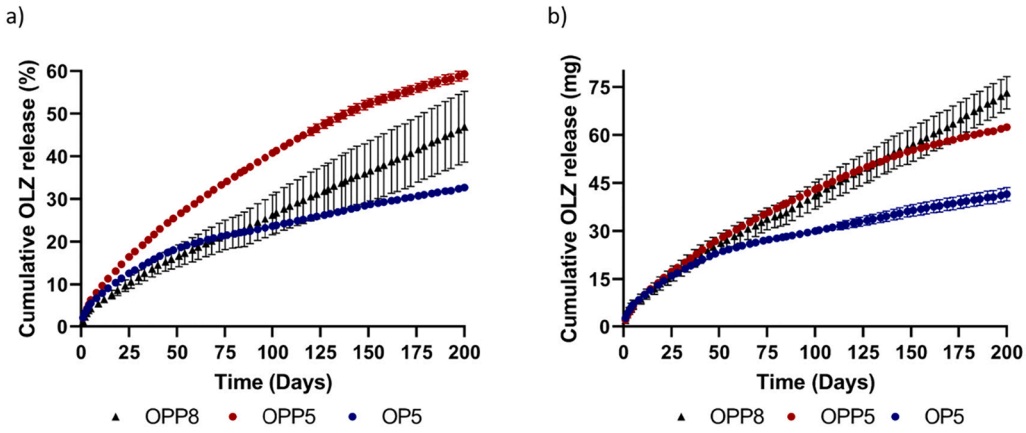

Fig. 6. Cumulative release of OLZ from the formulated implants presented as (a) percentage OLZ release and (b) actual mass of OLZ released. All results shown as means +/- S.D., n = 3.

new peaks were observed suggested that no chemical reactions occurred during implant manufacture.

The last technique used to characterise the implants was µCT. Fig. 5 shows images of the µCT analysis of the implants described in this work. When interpreting images from µCT analysis, areas of higher density, which are coloured white, are consistent with the presence of crystalline drug (Barrett et al., 2018; Turner et al., 2020). For OP5, OPP5 and OPP8, these areas of crystallinity are evenly distributed throughout the entire implant volume suggesting an even drug distribution. For the OPP8 sample areas of higher density are more prevalent indicating a higher quantity of incorporated drug. Therefore, these areas of higher intensity can be attributed to the presence of drug. When comparing OP5 and OPP5 it is obvious that there are slightly more areas of higher density within the material. This can be attributed to a higher presence of crystalline drug in this type of implants than in OPP5. These results are consistent with the results reported for DSC, TGA, XRD and FTIR analysis.

3.3. Drug release from implants

The release profiles of OLZ from the formulated implants are presented in Fig. 6. All formulations tested (OP5, OPP5 and OPP8) were capable of maintaining sustained release for a period of 200 days. At this point, the percentage of total OLZ content released was 32.74 %, 59.34 % and 49.44 % for OP5, OPP5 and OPP8 implants, respectively. Considering OP5 implants, an almost linear release profile was observed during the 50 days, after which drug release began to decrease gradually. The reduced overall drug release from OP5 when compared to OPP5 could be attributed to the higher proportion of crystalline OLP present within this formulation. The presence of PEG in OPP5 facilitated increased conversion of OLZ into an amorphous form which corresponded to enhanced drug solubility and, therefore, improved drug release into the aqueous media in which the implants were submerged. Another theory, and one that has been reported previously (Picco et al., 2022), is that PEG may act as a co-solvent in this instance.

Although OPP8 implants also contained PEG, they demonstrated reduced percentage drug release compared to OPP5 implants. This finding may be attributed to the increased drug loading which increases the proportion of crystalline and, therefore, poorly soluble OLZ present in these implants. Nevertheless, the drug release profile of OPP8 implants is substantially more linear than the other implant formulations tested. With this in mind, it is reasonable to suggest that this formulation may be well suited for further development as an implantable and long-acting drug delivery system.

Table 3
Results obtained after fitting OLZ release from OP5, OPP5 and OPP8 implants to Korsmeyer-Peppas model.

	Korsmeyer-Peppas		
	K_{KP} (day^{-n})	n	R^2
OP5	0.03005	0.4510	0.9969
OPP5	0.02450	0.6084	0.9978
OPP8	0.008715	0.7475	0.9971

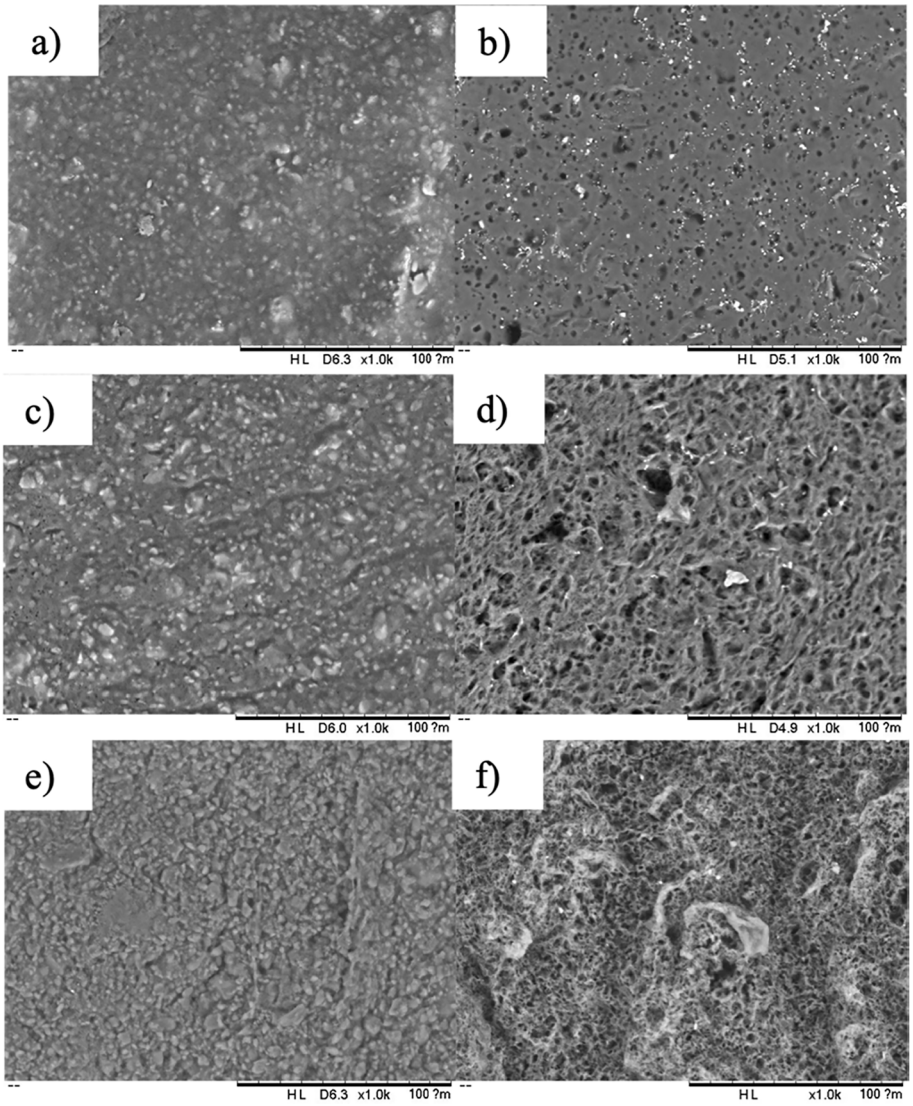

Fig. 7. Comparison of implants during drug release studies at x1000 magnification a) OP5 implant at day 0, b) OP5 implant at day 200, c) OPP5 implant at day 0 and d) OPP5 implant at day 200, e) OPP8 implant at day 0 and f) OPP8 implant at day 200. The scale in these images is 100 μm.

OLZ release from OP5, OPP5 and OPP8 implants was assessed using the Korsmeyer-Peppas mathematical model (Table 3). An "n" value of 0.45 in the Korsmeyer-Peppas model indicates that drug release from an implant is most likely *via* a mechanism of diffusion. This was the case in OP5 implants, which had an n value of 0.4510. These results suggested that the release of OLZ from these implants was governed by Fickian diffusion. PCL shows slow degradation kinetics as opposed to other biodegradable polymers such as PLGA (Lao et al., 2008). Therefore, it is not surprising that OLZ release kinetics are a result of drug diffusion rather than polymer degradation. These results are in line with previously reported drug delivery systems based on PCL (Lao et al., 2008; Utomo et al., 2022a). On the other hand, OPP5 and OPP8 implants presented a higher "n" value using the Korsmeyer-Peppas model (0.6084 and 0.7475, respectively). Values higher than 0.45 indicate drug release led by a combination of diffusion and erosion/relaxation of the implant matrix. These results suggest that there was some degree of matrix erosion/degradation involved in the release process. These results are not surprising considering that these implants contained PEG, a water-soluble polymer, in their structure. During the release process, this polymer will be released generating pores and contributing to the release process. SEM was used to analyse the surface of the implants after the release experiment (Fig. 7). These analyses demonstrated that PEG-containing implants (OPP5 and OPP8) possessed more porous structures after 200 days, when compared to OP5 implants. This supports the hypothesis that erosion was influential in drug release due to the presence of the water-soluble polymer PEG in implants.

This implantable system is presented as an alternative to the currently available marketed formulations. In this work, OLZ has been used as a model hydrophobic compound for the development of implantable long-acting drug delivery systems. Previous studies have focused on increasing the effective drug-load of implantable device-based therapies by inserting multiple devices (Karunakaran et al., 2021). However, the implants described within may circumvent the need for multiple implants due to the highly predictable and sustained manner of their drug release.

3.4. Cytocompatibility of implants

The polymers used in this work were selected in part due to the fact that they were both previously approved for human use by the FDA. Consequently, no cytocompatibility issues were expected to arise from the use of these polymers. However, DCM was used as a solvent to obtain printable polymeric solutions containing OLZ and it is well documented that high concentrations of DCM within a pharmaceutical product or

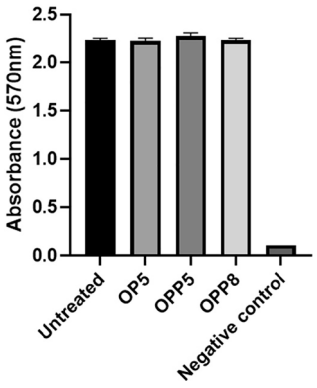

Fig. 8. Cytocompatibility test for OP5, OPP5 and OPP8 implants on HEK293T cells.

medical device may lead to a toxicity issues. Encouragingly, DCM has been extensively used for tablet coating for many years and it is also accepted by the FDA (FDA, 2017; Sohi et al., 2004). Nevertheless, it is imperative that DCM levels are controlled and maintained well below toxic levels in any product that is intended for human-use. Residual DCM content of the implants, which was measured using gas chromatography, revealed that all samples contained DCM levels below 50 ppm. Considering that the FDA acceptable maximum level is 600 ppm it can be concluded that the resulting implants are compliant with this requirement (FDA, 2017). Despite this low solvent content, a cytocompatibility study was carried out using HEK293T cell line to extensively characterise the safety of these implants. This cell line has been used previously to evaluate the cytocompatibility of medical devices and pharmaceutical formulations (Avti et al., 2013; Burugapalli et al., 2016; Picco et al., 2022). Implants were treated with cells for a period of 7 days, with MTT assays carried out as described previously at day 7. After evaluating the results showed in Fig. 8 and use a one-way ANOVA statistical test it can be concluded that the samples are not cytotoxic, which supports the hypothesis that the formulated implants are safe for use.

4. Conclusion

This work has demonstrated the usefulness of 3D-printing technology in the formulation of implants for long-acting delivery. Three different candidate implant formulations, containing OLZ, PCL and PEG at varying concentrations, were successfully developed and manufactured using a robocasting 3D printer. Visual and physicochemical characterisation of these implants indicated suitable product homogeneity. Additionally, physicochemical characterisation of the implants indicated no chemical alteration of the API during the manufacturing process. Drug/polymer interactions were identified and characterised using DSC, XRD, TGA and FTIR techniques and used to estimate the crystallinity of OLZ in the formulated implants. All implants tested demonstrated the ability to slowly release OLZ over a period of 200 days. Particularly, PCL and PEG based implants with 80 % drug loading (OPP8), which exhibited an almost linear release profile after the first 25 days of release. The use of DCM for implant preparation is potentially problematic as regulatory bodies have restricted residual levels of this compound to 600 ppm (FDA, 2017). Analysis using gas chromatography revealed that, in their final form, all of the formulated implants contained no more than 50 ppm DCM. This finding, in combination with positive cytocompatibility results, suggested that these implants are likely to be safe for human use. Undoubtedly, further studies, such as *in vivo* experimentation using appropriate animal models and optimisation of terminal sterilisation strategies, are required to ensure this. Finally, multiple regulatory queries regarding the use of 3D-printing for the production of personalised point-of-care therapeutics remain unanswered at this time. Unquestionably, these hurdles must be overcome before implants, such as those reported here, receive market authorisation and beneficially impact the lives of patients on a global scale. Encouragingly, recent efforts by various stakeholders within the field of implantable therapeutics has accelerated the development of new guidance to solve this issue and many others. It is hoped that continued collaborative endeavours in line with this regulatory theme may aid significantly the translation of this technology to the market.

Disclosure statement.

No potential conflict of interest was reported by the author(s).

CRediT authorship contribution statement

Camila J. Picco: Conceptualization, Data curation, Formal analysis, Investigation, Methodology, Validation, Writing – original draft, Writing – review & editing. **Emilia Utomo:** Data curation, Conceptualization, Formal analysis, Investigation, Writing – review & editing. **Andrea McClean:** Data curation, Formal analysis, Conceptualization, Investigation. **Juan Domínguez-Robles:** Investigation, Writing – original draft, Writing – review & editing. **Qonita Kurnia Anjani:** Data curation, Investigation, Writing – review & editing. **Fabiana Volpe-Zanutto:** Data curation, Investigation, Writing – review & editing. **Peter E. McKenna:** Writing – original draft, Writing – review & editing. **Jonathan Acheson:** Investigation, Methodology. **Dessislava Malinova:** Data curation, Investigation, Methodology. **Ryan F. Donnelly:** Supervision, Resources, Funding acquisition, Writing – original draft, Writing – review & editing. **Eneko Larrañeta:** Conceptualization, Supervision, Resources, Funding acquisition, Writing – original draft, Writing – review & editing.

Declaration of Competing Interest

The authors declare that they have no known competing financial interests or personal relationships that could have appeared to influence the work reported in this paper.

Data availability

The authors are unable or have chosen not to specify which data has been used.

Acknowledgments

The authors thank the Academy of Medical Sciences (SBF005\1011) and the Royal Society (RGS\R2\212016) for the financial support to this work and Gina L. Picco for her support in providing and designing the illustrations included in the graphical abstract of this manuscript. Finally, the authors thank Prof. P. Manesiotis for aiding the determination of residual solvent content.

References

Anjani, Q.K., Domínguez-Robles, J., Utomo, E., Font, M., Martínez-Ohárriz, M.C., Permana, A.D., Cárcamo-Martínez, Á., Larrañeta, E., Donnelly, R.F., 2022. Inclusion Complexes of Rifampicin with Native and Derivatized Cyclodextrins: In Silico Modeling, Formulation, and Characterization. Pharm. https://doi.org/10.3390/ph15010020.

Avti, P.K., Caparelli, E.D., Sitharaman, B., 2013. Cytotoxicity, cytocompatibility, cell-labeling efficiency, and in vitro cellular magnetic resonance imaging of gadolinium-catalyzed single-walled carbon nanotubes. J. Biomed. Mater. Res. Part A 101, 3580–3591. https://doi.org/10.1002/jbm.a.34643.

Awad, A., Fina, F., Goyanes, A., Gaisford, S., Basit, A.W., 2020. 3D printing: Principles and pharmaceutical applications of selective laser sintering. Int. J. Pharm. 586, 119594 https://doi.org/10.1016/j.ijpharm.2020.119594.

Barrett, S.E., Teller, R.S., Forster, S.P., Li, L., Mackey, M.A., Skomski, D., Yang, Z., Fillgrove, K.L., Doto, G.J., Wood, S.L., Lebron, J., Grobler, J.A., Sanchez, R.I., Liu, Z., Lu, B., Niu, T., Sun, L., Gindy, M.E., 2018. Extended-duration MK-8591-eluting implant as a candidate for HIV treatment and prevention. Antimicrob. Agents Chemother. 62 https://doi.org/10.1128/AAC.01058-18.

Bassand, C., Freitag, J., Benabed, L., Verin, J., Siepmann, F., Siepmann, J., 2022. PLGA implants for controlled drug release: Impact of the diameter. Eur. J. Pharm. Biopharm. 177, 50–60. https://doi.org/10.1016/j.ejpb.2022.05.020.

Boia, R., Dias, P.A.N., Martins, J.M., Galindo-Romero, C., Aires, I.D., Vidal-Sanz, M., Agudo-Barriuso, M., de Sousa, H.C., Ambrósio, A.F., Braga, M.E.M., Santiago, A.R., 2019. Porous poly(ε-caprolactone) implants: a novel strategy for efficient intraocular drug delivery. J. Control. Release 316, 331–348. https://doi.org/10.1016/j.jconrel.2019.09.023.

Burugapalli, K., Razavi, M., Zhou, L., Huang, Y., 2016. In vitro cytocompatibility study of a medical β-Type Ti-35.5Nb-5.7Ta titanium alloy. J. Biomater. Tissue Eng. 6, 141–148. https://doi.org/10.1166/jbt.2016.1424.

Cailleaux, S., Sanchez-Ballester, N.M., Gueche, Y.A., Bataille, B., Soulairol, I., 2021. Fused deposition modeling (FDM), the new asset for the production of tailored medicines. J. Control. Release 330, 821–841. https://doi.org/10.1016/j.jconrel.2020.10.056.

Champeau, M., Thomassin, J.-M., Tassaing, T., Jérôme, C., 2015. Drug loading of polymer implants by supercritical CO2 assisted impregnation: a review. J. Control. Release 209, 248–259. https://doi.org/10.1016/j.jconrel.2015.05.002.

Corduas, F., Mancuso, E., Lamprou, D.A., 2020. Long-acting implantable devices for the prevention and personalised treatment of infectious, inflammatory and chronic diseases. J. Drug Deliv. Sci. Technol. 60, 101952 https://doi.org/10.1016/j.jddst.2020.101952.

Costa, P., Sousa Lobo, J.M., 2003. Evaluation of mathematical models describing drug release from estradiol transdermal systems. Drug Dev. Ind. Pharm. 29, 89–97. https://doi.org/10.1081/DDC-120016687.

Cutler, R.L., Fernandez-Llimos, F., Frommer, M., Benrimoj, C., Garcia-Cardenas, V., 2018. Economic impact of medication non-adherence by disease groups: a systematic review. BMJ Open 8, e016982.

Danafar, H., Davaran, S., Rostamizadeh, K., Valizadeh, H., Hamidi, M., 2014. Biodegradable m-PEG/PCL core-shell micelles: preparation and characterization as a sustained release formulation for curcumin. Adv. Pharm. Bull. 4, 501–510. https://doi.org/10.5681/apb.2014.074.

Domínguez-Robles, J., Mancinelli, C., Mancuso, E., García-Romero, I., Gilmore, B.F., Casettari, L., Larrañeta, E., Lamprou, D.A., 2020. 3D printing of drug-loaded thermoplastic polyurethane meshes: a potential material for soft tissue reinforcement in vaginal surgery. Pharmaceutics 12, 63. https://doi.org/10.3390/pharmaceutics12010063.

Domínguez-Robles, J., Diaz-Gomez, L., Utomo, E., Shen, T., Picco, C.J., Alvarez-Lorenzo, C., Concheiro, A., Donnelly, R.F., Larrañeta, E., 2021a. Use of 3D printing for the development of biodegradable antiplatelet materials for cardiovascular applications. Pharmaceuticals 14, 921. https://doi.org/10.3390/ph14090921.

Domínguez-Robles, J., Shen, T., Cornelius, V.A., Corduas, F., Mancuso, E., Donnelly, R.F., Margariti, A., Lamprou, D.A., Larrañeta, E., 2021b. Development of drug loaded cardiovascular prosthesis for thrombosis prevention using 3D printing. Mater. Sci. Eng. C 129, 112375. https://doi.org/10.1016/j.msec.2021.112375.

Domínguez-Robles, J., Utomo, E., Cornelius, V.A., Anjani, Q.K., Korelidou, A., Gonzalez, Z., Donnelly, R.F., Margariti, A., Delgado-Aguilar, M., Tarrés, Q., Larrañeta, E., 2022. TPU-based antiplatelet cardiovascular prostheses prepared using fused deposition modelling. Mater. Des. 220, 110837 https://doi.org/10.1016/j.matdes.2022.110837.

Domsta, V., Seidlitz, A., 2021. 3D-printing of drug-eluting implants: an overview of the current developments described in the literature. Mol. https://doi.org/10.3390/molecules26134066.

Elamparithi, A., Ravi, M., Balachandran, C., Rao, S., Paul, S.F., 2016. Biocompatibility Evaluation of Electrospun Collagen , Gelatin , Polycaprolactone and their Composite Matrices in Rattus Norvegicus.

Ethylene oxide sterilization: how hospitals can adapt to the changes., 1994. . Health Devices 23, 485–92.

Farmer, Z.-L., Domínguez-Robles, J., Mancinelli, C., Larrañeta, E., Lamprou, D.A., 2020. Urogynecological surgical mesh implants: new trends in materials, manufacturing and therapeutic approaches. Int. J. Pharm. 585, 119512 https://doi.org/10.1016/j.ijpharm.2020.119512.

Farmer, Z.-L., Utomo, E., Domínguez-Robles, J., Mancinelli, C., Mathew, E., Larrañeta, E., Lamprou, D.A., 2021. 3D printed estradiol-eluting urogynecological mesh implants: influence of material and mesh geometry on their mechanical properties. Int. J. Pharm. 593, 120145 https://doi.org/10.1016/j.ijpharm.2020.120145.

Fda, 2017. Q3C — Tables and List Guidance for Industry. Microsoft Word 9765, 1–8.

Fialho, S.L., da Silva Cunha, A., 2005. Manufacturing techniques of biodegradable implants intended for intraocular application. Drug Deliv. 12, 109–116. https://doi.org/10.1080/10717540590921432.

Funk, S., Miller, M.M., Mishell, D.R., Archer, D.F., Poindexter, A., Schmidt, J., Zampaglione, E., 2005. Safety and efficacy of Implanon™, a single-rod implantable contraceptive containing etonogestrel. Contraception 71, 319–326. https://doi.org/10.1016/j.contraception.2004.11.007.

Higashi, K., Medic, G., Littlewood, K.J., Diez, T., Granstrom, O., De Hert, M., 2013. Medication adherence in schizophrenia: factors influencing adherence and consequences of nonadherence, a systematic literature review. Ther. Adv. Psychopharmacol. 3, 200–218. https://doi.org/10.1177/2045125312474019 [doi].

Hiriyanna, S.G., Basavaiah, K., Goud, P.S.K., Dhayanithi, V., Raju, K., Pati, H.N., 2008. Identification and characterization of olanzapine degradation products under oxidative stress conditions. Acta Chromatogr. 20, 81–93. https://doi.org/10.1556/AChrom.20.2008.1.7.

Kabirian, F., Ditkowski, B., Zamanian, A., Heying, R., Mozafari, M., 2018. An innovative approach towards 3D-printed scaffolds for the next generation of tissue-engineered vascular grafts. Mater. Today Proc. 5, 15586–15594. https://doi.org/10.1016/j.matpr.2018.04.167.

Karunakaran, D., Simpson, S.M., Su, J.T., Bryndza-Tfaily, E., Hope, T.J., Veazey, R., Dobek, G., Qiu, J., Watrous, D., Sung, S., Chacon, J.E., Kiser, P.F., 2021. Design and testing of a cabotegravir implant for HIV prevention. J. Control. Release 330, 658–668. https://doi.org/10.1016/j.jconrel.2020.12.024.

Khaled, S.A., Burley, J.C., Alexander, M.R., Roberts, C.J., 2014. Desktop 3D printing of controlled release pharmaceutical bilayer tablets. Int. J. Pharm. 461, 105–111. https://doi.org/10.1016/j.ijpharm.2013.11.021.

Khaled, S.A., Alexander, M.R., Irvine, D.J., Wildman, R.D., Wallace, M.J., Sharpe, S., Yoo, J., Roberts, C.J., 2018a. Extrusion 3D printing of paracetamol tablets from a single formulation with tunable release profiles through control of tablet geometry. AAPS PharmSciTech 19, 3403–3413. https://doi.org/10.1208/s12249-018-1107-z.

Khaled, S.A., Alexander, M.R., Wildman, R.D., Wallace, M.J., Sharpe, S., Yoo, J., Roberts, C.J., 2018b. 3D extrusion printing of high drug loading immediate release paracetamol tablets. Int. J. Pharm. 538, 223–230. https://doi.org/10.1016/j.ijpharm.2018.01.024.

Kleinsinger, F., 2018. The unmet challenge of medication nonadherence. Perm. J. 22, 18–33. https://doi.org/10.7812/TPP/18-033.

Korelidou, A., Domínguez-Robles, J., Magill, E., Eleftheriadou, M., Cornelius, V.A., Donnelly, R.F., Margariti, A., Larrañeta, E., 2022. 3D-printed reservoir-type implants containing poly(lactic acid)/poly(caprolactone) porous membranes for sustained drug delivery. Biomater. Adv. 213024 https://doi.org/10.1016/j.bioadv.2022.213024.

Kyle, S., Jessop, Z.M., Al-Sabah, A., Whitaker, I.S., 2017. Printability'' of candidate biomaterials for extrusion based 3D printing: state-of-the-art. Adv. Healthc. Mater. 6, 1700264. https://doi.org/10.1002/adhm.201700264.

Lao, L.L., Venkatraman, S.S., Peppas, N.A., 2008. Modeling of drug release from biodegradable polymer blends. Eur. J. Pharm. Biopharm. 70, 796–803. https://doi.org/10.1016/j.ejpb.2008.05.024.

Larrañeta E., Singh T.R.R. and Donnelly R.F., 2021. Long-Acting Drug Delivery Systems Pharmaceutical, Clinical, and Regulatory Aspects, 1st ed. https://doi.org/10.1016/C2019-0-03097-X.

Larrañeta, E., Singh, T.R.R., & Donnelly, R.F., 2022. Overview of the clinical current needs and potential applications for long-acting and implantable delivery systems. In E. Larrañeta, T. R. R. Singh, & R. F. Donnelly (Eds.), Long-acting drug delivery systems: pharmaceutical, clinical, and regulatory aspects (pp. 1-16). (Woodhead Publishing Series in Biomaterials). Woodhead Publishing. https://doi.org/10.1016/B978-0-12-821749-8.00005-7.

Larrañeta, E., Martínez-Ohárriz, C., Vélaz, I., Zornoza, A., Machín, R., Isasi, J.R., 2014. In Vitro release from reverse poloxamine/α-cyclodextrin matrices: modelling and comparison of dissolution profiles. J. Pharm. Sci. 103, 197–206. https://doi.org/10.1002/jps.23774.

León, A., Reuquen, P., Garín, C., Segura, R., Vargas, P., Zapata, P., Orihuela, P.A., 2017. FTIR and Raman characterization of TiO2 nanoparticles coated with polyethylene glycol as carrier for 2-methoxyestradiol. Appl. Sci. https://doi.org/10.3390/app7010049.

Liaskoni, A., Wildman, R.D., Roberts, C.J., 2021. 3D printed polymeric drug-eluting implants. Int. J. Pharm. 597, 120330 https://doi.org/10.1016/j.ijpharm.2021.120330.

Lopez-Vidal, L., Real, J.P., Real, D.A., Camacho, N., Kogan, M.J., Paredes, A.J., Palma, S.D., 2022. Nanocrystal-based 3D-printed tablets: semi-solid extrusion using melting solidification printing process (MESO-PP) for oral administration of poorly soluble drugs. Int. J. Pharm. 611, 121311 https://doi.org/10.1016/j.ijpharm.2021.121311.

Martin, N.K., Domínguez-Robles, J., Stewart, S.A., Cornelius, V.A., Anjani, Q.K., Utomo, E., García-Romero, I., Donnelly, R.F., Margariti, A., Lamprou, D.A., Larrañeta, E., 2021. Fused deposition modelling for the development of drug loaded cardiovascular prosthesis. Int. J. Pharm. 595, 120243 https://doi.org/10.1016/j.ijpharm.2021.120243.

Melchiorri, A.J., Hibino, N., Best, C.A., Yi, T., Lee, Y.U., Kraynak, C.A., Kimerer, L.K., Krieger, A., Kim, P., Breuer, C.K., Fisher, J.P., 2016. 3D-printed biodegradable polymeric vascular grafts. Adv. Healthc. Mater. 5, 319–325. https://doi.org/10.1002/adhm.201500725.

Melocchi, A., Uboldi, M., Cerea, M., Foppoli, A., Maroni, A., Moutaharrik, S., Palugan, L., Zema, L., Gazzaniga, A., 2020. A graphical review on the escalation of fused deposition modeling (FDM) 3D printing in the pharmaceutical field. J. Pharm. Sci. 109, 2943–2957. https://doi.org/10.1016/j.xphs.2020.07.011.

Pandey, M., Choudhury, H., Fern, J.L.C., Kee, A.T.K., Kou, J., Jing, J.L.J., Her, H.C., Yong, H.S., Ming, H.C., Bhattamisra, S.K., Gorain, B., 2020. 3D printing for oral drug delivery: a new tool to customize drug delivery. Drug Deliv. Transl. Res. 10, 986–1001. https://doi.org/10.1007/s13346-020-00737-0.

Picco, C.J., Domínguez-Robles, J., Utomo, E., Paredes, A.J., Volpe-Zanutto, F., Malinova, D., Donnelly, R.F., Larrañeta, E., 2022. 3D-printed implantable devices with biodegradable rate-controlling membrane for sustained delivery of hydrophobic drugs. Drug Deliv. 29, 1038–1048. https://doi.org/10.1080/10717544.2022.2057620.

Pina, M.F., Zhao, M., Pinto, J.F., Sousa, J.J., Craig, D.Q.M., 2014. The influence of drug physical state on the dissolution enhancement of solid dispersions prepared via hot-melt extrusion: a case study using olanzapine. J. Pharm. Sci. 103, 1214–1223. https://doi.org/10.1002/jps.23894.

Quarterman, J.C., Geary, S.M., Salem, A.K., 2021. Evolution of drug-eluting biomedical implants for sustained drug delivery. Eur. J. Pharm. Biopharm. 159, 21–35. https://doi.org/10.1016/j.ejpb.2020.12.005.

Ritger, P.L., Peppas, N., 1987. A simple equation for description of solute release I. Fickian and Non-Fickian release from non-swellable devices in the form of slabs,

spheres, cylinders or discs. J. Control. Release 5, 23–36. https://doi.org/10.1016/0168-3659(87)90034-4.

Ruiz-Cantu, L., Trindade, G.F., Taresco, V., Zhou, Z., He, Y., Burroughs, L., Clark, E.A., Rose, F.R.A.J., Tuck, C., Hague, R., Roberts, C.J., Alexander, M., Irvine, D.J., Wildman, R.D., 2022. Correction to "bespoke 3D-printed polydrug implants created via microstructural control of oligomers". ACS Appl. Mater. Interfaces 14, 8654. https://doi.org/10.1021/acsami.2c00035.

Seoane-Viaño, I., Ong, J.J., Luzardo-Álvarez, A., González-Barcia, M., Basit, A.W., Otero-Espinar, F.J., Goyanes, A., 2021. 3D printed tacrolimus suppositories for the treatment of ulcerative colitis. Asian J. Pharm. Sci. 16, 110–119. https://doi.org/10.1016/j.ajps.2020.06.003.

Serrano, M.C., Pagani, R., Vallet-Regí, M., Peña, J., Rámila, A., Izquierdo, I., Portolés, M. T., 2004. In vitro biocompatibility assessment of poly(ε-caprolactone) films using L929 mouse fibroblasts. Biomaterials 25, 5603–5611. https://doi.org/10.1016/j.biomaterials.2004.01.037.

Sohi, H., Sultana, Y., Khar, R.K., 2004. Taste masking technologies in oral pharmaceuticals: recent developments and approaches. Drug Dev. Ind. Pharm. 30, 429–448.

Stewart, S., Domínguez-Robles, J., McIlorum, V., Mancuso, E., Lamprou, D., Donnelly, R., Larrañeta, E., 2020a. Development of a biodegradable subcutaneous implant for prolonged drug delivery using 3D printing. Pharmaceutics 12, 105. https://doi.org/10.3390/pharmaceutics12020105.

Stewart, S.A., Domínguez-Robles, J., McIlorum, V.J., Gonzalez, Z., Utomo, E., Mancuso, E., Lamprou, D.A., Donnelly, R.F., Larrañeta, E., 2020b. Poly (caprolactone)-based coatings on 3D-printed biodegradable implants: a novel strategy to prolong delivery of hydrophilic drugs. Mol. Pharm. 17, 3487–3500. https://doi.org/10.1021/acs.molpharmaceut.0c00515.

Stewart, S.A., Domínguez-Robles, J., Utomo, E., Picco, C.J., Corduas, F., Mancuso, E., Amir, M.N., Bahar, M.A., Sumarheni, S., Donnelly, R.F., Permana, A.D., Larrañeta, E., 2021. Poly(caprolactone)-based subcutaneous implant for sustained delivery of levothyroxine. Int. J. Pharm. 607, 121011 https://doi.org/10.1016/j.ijpharm.2021.121011.

Teoh, J.H., Mozhi, A., Sunil, V., Tay, S.M., Fuh, J., Wang, C., 2021. 3D printing personalized, photocrosslinkable hydrogel wound dressings for the treatment of thermal burns. Adv. Funct. Mater. 31, 2105932. https://doi.org/10.1002/adfm.202105932.

Tian, P., Yang, F., Xu, Y., Lin, M.-M., Yu, L.-P., Lin, W., Lin, Q.-F., Lv, Z.-F., Huang, S.-Y., Chen, Y.-Z., 2018. Oral disintegrating patient-tailored tablets of warfarin sodium produced by 3D printing. Drug Dev. Ind. Pharm. 44, 1918–1923. https://doi.org/10.1080/03639045.2018.1503291.

Turner, T.D., Gajjar, P., Fragkopoulos, I.S., Carr, J., Nguyen, T.T.H., Hooper, D., Clarke, F., Dawson, N., Withers, P.J., Roberts, K.J., 2020. Measuring the particle packing of <scp>l</scp> -glutamic acid crystals through X-ray computed tomography for understanding powder flow and consolidation behavior. Cryst. Growth Des. 20, 4252–4263. https://doi.org/10.1021/acs.cgd.9b01515.

Utomo, E., Domínguez-Robles, J., Moreno-Castellanos, N., Stewart, S.A., Picco, C.J., Anjani, Q.K., Simón, J.A., Peñuelas, I., Donnelly, R.F., Larrañeta, E., 2022a. Development of intranasal implantable devices for schizophrenia treatment. Int. J. Pharm. 624, 122061 https://doi.org/10.1016/j.ijpharm.2022.122061.

Utomo, E., Stewart, S.A., Picco, C.J., Domínguez-Robles, J., Larrañeta, E., 2022b. Classification, material types, and design approaches of long-acting and implantable drug delivery systems, in: Long-Acting Drug Delivery Systems. Elsevier, pp. 17–59. https://doi.org/10.1016/B978-0-12-821749-8.00012-4.

Vaz, V.M., Kumar, L., 2021. 3D printing as a promising tool in personalized medicine. AAPS PharmSciTech 22, 49. https://doi.org/10.1208/s12249-020-01905-8.

Volpe-Zanutto, F., Ferreira, L.T., Permana, A.D., Kirkby, M., Paredes, A.J., Vora, L.K., P. Bonfanti, A., Charlie-Silva, I., Raposo, C., Figueiredo, M.C., Sousa, I.M.O., Brisibe, A., Costa, F.T.M., Donnelly, R.F., Foglio, M.A., 2021. Artemether and lumefantrine dissolving microneedle patches with improved pharmacokinetic performance and antimalarial efficacy in mice infected with Plasmodium yoelii. J. Control. Release 333, 298–315. https://doi.org/10.1016/j.jconrel.2021.03.036.